ARTICLE

Quantum Confinement, Surface Roughness, and the Conduction Band Structure of Ultrathin Silicon Membranes

Feng Chen,[†,‡,⊥] Edwin B. Ramayya,[†,⊥] Chanan Euaruksakul,[†] Franz J. Himpsel,[†] George K. Celler,[§] Bingjun Ding,[‡] Irena Knezevic,[†] and Max G. Lagally[†,*]

[†]University of Wisconsin-Madison, Madison, Wisconsin 53706, [‡]Xi'an Jiaotong University, Xi'an, Shannxi 710049, China, and [§]Soitec USA, 2 Centennial Drive, Peabody, Massachusetts 01960. [⊥]These authors contributed equally to the work.

ABSTRACT We report direct measurements of changes in the conduction-band structure of ultrathin silicon nanomembranes with quantum confinement. Confinement lifts the 6-fold-degeneracy of the bulk-silicon conduction-band minimum (CBM), Δ, and two inequivalent sub-band ladders, Δ_2 and Δ_4, form. We show that even very small surface roughness smears the nominally steplike features in the density of states (DOS) due to these sub-bands. We obtain the energy splitting between Δ_2 and Δ_4 and their shift with respect to the bulk value directly from the $2p_{3/2} \rightarrow \Delta$ transition in X-ray absorption. The measured dependence of the sub-band splitting and the shift of their weighted average on degree of confinement is in excellent agreement with theory, for both Si(001) and Si(110).

KEYWORDS: silicon nanomembrane · quantum confinement · surface roughness · thermoelectric · valley splitting

When electrons in a crystalline solid are confined to a region smaller than the typical carrier de Broglie wavelength, the electronic band structure is modified.[1] This phenomenon, known as quantum confinement, causes the transport and optical properties of charge carriers to be different from those in bulk material. It is an essential aspect of the electronic properties of small nanowires and nanoparticles.[2] Quantum confinement introduces changes in the DOS, inducing shifts and degeneracy splitting in features of the band structure. Changes of this nature occurring in the conduction band of semiconductors can significantly affect level occupancy, interband transitions, and the density and mobility of conducting electrons.[3]

In addition, at these nanodimensions, variations in thickness in the confinement direction(s), for example due to surface roughness, can alter the ideal DOS expected from confinement, causing states to be broadened and transport to be affected.

We demonstrate here the influence of quantum confinement on the conduction band structure of silicon, using very thin Si slabs and a combination of spectroscopy and theory, and we elucidate the effect of surface roughness on the confinement-modified band structure. Why investigate these properties in silicon? Apart from its technological relevance and the fact that it is the model system for an indirect-band gap semiconductor, recent studies have placed Si in the limelight as a potentially useful thermoelectric material when it is fabricated in the form of nanowires. It was shown that, for 20−50 nm diameter nanowires, the thermoelectric figure of merit could be increased up to two orders or magnitude *via* the reduction of thermal conductivity.[4,5] Specifically, surface roughness of the nanowires contributes significantly to the phonon scattering and thus the increase in the figure of merit, *ZT*, which is inversely dependent on the thermal conductivity and directly dependent on the electrical conductivity and the thermopower of the material.[4−6]

The dramatic increase in *ZT* in Si obtained at nanodimensions, along with the pervasiveness of Si in all manner of technology, makes it imperative to explore all avenues to improve further the thermoelectric properties of Si.[5] In addition to efforts at further reduction in thermal conductivity, one can address increasing the thermopower *via* increases in the electrical conductivity. A number of years ago it was proposed that,[7] if the discrete sub-bands that form due to quantum confinement in the electronic band structure of quantum wells and wires are positioned properly with respect to the Fermi level,[6,7] one could observe an enhanced *ZT*. In this scenario, the sharpness of features in the lower-dimensionality DOS is quite important. Any factors that could broaden these features,

*Address correspondence to lagally@engr.wisc.edu.

Received for review February 9, 2010 and accepted March 13, 2010.

Published online March 19, 2010. 10.1021/nn100275z

such as variation in the quantum well thickness, may negate the benefits. We approach this problem in Si by investigating first the quantum size effect for confinement in one dimension, something that is quantifiably achievable, and then projecting the results to confinement in two dimensions (i.e., nanowires). We explicitly include surface roughness, which proves to be of paramount importance in diminishing benefits from quantum confinement.

We introduce here the optimal system for direct investigations of 1D confinement in Si, the outer (template) layer of Si in silicon-on-insulator (SOI). This layer, with a specific orientation, such as (001) or (110), can be thinned to 1−2 nm, while maintaining perfect crystallinity laterally over the size of a wafer. This simple, well-defined slab geometry, providing 1D confinement in *z* and no confinement in *x* or *y*, is ideal both for clarity in the measurement and for testing theoretical models. We report direct measurements and calculations of the influence of thickness on the shift and the splitting of the conduction band minima in very thin, unstrained single-crystal Si membranes with two surface orientations, (001) and (110). We fabricate Si sheets as thin as 1.3 nm (~10 atomic layers). Si has a thermal de Broglie wavelength of ~12 nm at room temperature, and therefore we are well within the quantum confinement limit. We use high-energy-resolution soft-X-ray absorption spectroscopy (XAS) with total electron yield (TEY) detection. XAS in the TEY mode has very high surface sensitivity, originating from the shallow escape depth of secondary electrons.[8] XAS is therefore an effective tool to investigate directly changes in the Si conduction band for very thin sheets.[9] We measure splitting of the degenerate states of the CBM (the Δ valley) as large as 260 meV for the thinnest Si(001) samples and changes in the 2*p*-to-conduction band transition energy (average Δ valley shift) as large as 150 meV. We demonstrate, by comparison with theory, the significance of surface roughness on conduction band structure in the quantum confinement limit, and on the observable XAS spectra.

No prior direct measurements of the influence of confinement on conduction band structure exist on thin, crystalline Si nanomembranes. Measurements that do exist, on nanoparticles or polycrystalline/amorphous thin layers, are difficult to interpret.[10] For nanoparticles (and therefore 3D confinement),[11] size, shape, and orientation dispersion, surface termination, surface relaxation, and possible substrate interactions make the measurement of the effect of confinement on the band structure simply not possible. In the limited measurements on superlattices of poly(nano)crystalline/amorphous Si and SiO_2,[10,12] the confinement is nominally 1D, but the Si films consist of very small, differently sized, poorly oriented crystals and thus these films must resemble the nanoparticles of ref 10 in their behavior. In addition, no direct measurements exist at all on the splitting of the CBM with increased confinement, as such experiments require good crystals.

We create 1D confined Si by thinning the template layer of SOI, with either (001) or (110) orientation. SOI consists of thin crystalline Si (sometimes called the template layer, here synonymously referred to as membrane) separated by a SiO_2 layer from a thick bulk Si handling substrate. Membranes with thicknesses as low as 1.3 nm and as high as several hundred nm are fabricated (see Methods). The rms surface roughness (measured over 5 μm × 5 μm regions) of nanomembranes thin enough to be in the quantum size limit (<10 nm) is as low as 0.27 nm and below 0.4 nm for all samples, uniformly in all areas. The roughness, in comparison, of bulk Si(001) and amorphous Si, is 0.18 and 0.67 nm, respectively (see Methods).

We use linearly polarized monochromatic synchrotron radiation with 10 meV energy resolution to make the XAS measurements. Details of the XAS method can be found in prior work.[13] We sweep the photon energy and measure the total-electron-yield current to obtain the absorption spectra. The size of the beam on the sample is 4 μm × 16 μm, so the AFM-measured roughness of the nanomembranes is a good approximation to the beam-averaged roughness. We bracketed all sample scans with bulk-Si reference measurements to calibrate the energy scale of every spectrum to the L_{III} edge of unstrained Si, known to be at 99.85 eV.[14]

RESULTS AND DISCUSSION

We differentiate the measured X-ray absorption curves[15] and apply 21-point second-order Savitzky−Golay smoothing.[16] The steplike onsets of absorption edges become well-defined peaks. Representative results are shown in Figure 1. Derivative XAS spectra of the bulk Si reference show a sharp peak at 99.85 eV, the optical transition from the Si $2p_{3/2}$ core level to the CBM, which is degenerate (Δ_6) if the membrane is thick, and splits into Δ_2 and Δ_4 sub-bands if the membrane is thin enough. The spectra also show higher-order features at 100.82 and 102.59 eV, the transitions to L_1 and L_3 conduction band valleys, respectively.[17] These latter transitions are found in all crystalline-Si samples but are absent in noncrystalline Si because of the disorder scattering.[18,19] The spin−orbit splitting of the Si 2p core level generates two peaks for each transition. We can use the peak position of either to determine the transition energy change with increased quantum confinement. As the thicknesses decrease, the 2p → Δ transition shifts to higher energies for both SOI(110) and SOI(001).[11,19]

In an ultrathin Si membrane, potential barriers, due to oxide or free-surface termination, effectively confine the conduction-band electrons, making the membrane a quantum well in the confinement direction. The diminished long-range order in the direction perpendicular to the sample surface results in the formation of 2D

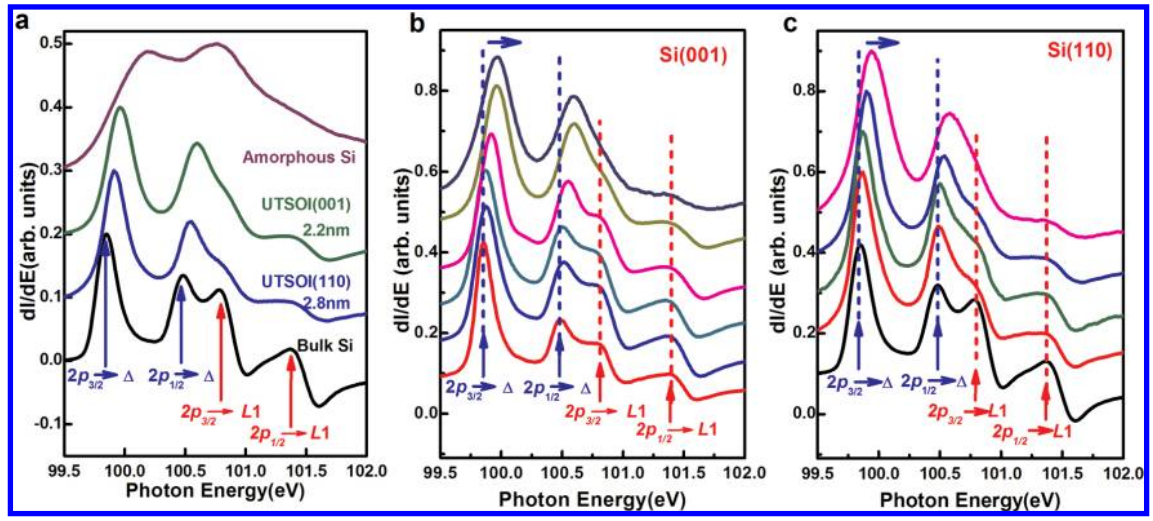

Figure 1. (a) Representative derivative X-ray absorption spectra showing the effect of quantum confinement on the conduction band structure of a thin Si membrane, for two orientations, compared with bulk crystalline Si and amorphous Si. The 2p→Δ transition shifts to higher energy as thickness decreases. Amorphous Si has no features at the 2p→L_1 transitions. The spin−orbit splitting of the 2p core level into $2p_{3/2}$ and $2p_{1/2}$ duplicates all peaks in the spectra. The curves are vertically offset for clarity. Spectra (b) show the peak position shifts in SOI(001). From bottom to top the curves represent membrane thicknesses of 6.6 nm, 4.1 nm, 3.9 nm, 3.2 nm, 2.2 nm, and 1.7 nm and (c) show the peak position shifts in SOI(110), with membrane thicknesses from bottom to top of 20, 5.6, 4.8, 2.8, and 1.3 nm.

sub-bands in each of the 6-fold degenerate valleys of bulk Si (Δ_6). The CBM associated with each valley bottom is now effectively shifted upward by the ground-sub-band energy, which is inversely proportional to the effective mass along the direction of confinement for the given valley. Confinement in either the ⟨001⟩ or the ⟨110⟩ direction splits the degeneracy of Δ_6 into 2-fold-degenerate Δ_2 valleys and 4-fold-degenerate Δ_4 valleys. For confinement along ⟨001⟩, Δ_2 represents the out-of-plane valleys and Δ_4 represents the in-plane valleys, with Δ_4 lying in energy above Δ_2. For confinement along ⟨110⟩, Δ_2 represents the in-plane valleys, and Δ_4 represents the valleys that contain out-of-plane components, with Δ_4 lying in energy below Δ_2.

We determine the shifting and splitting of the conduction band minima due to the 1D confinement by using the components (Δ_2 and Δ_4) of bulk Si in the ratio of their DOS. To confirm that this approach is correct, we perform calculations on a structure that models SOI nanomembranes, a sheet with carriers spatially confined in the direction perpendicular to the surface. The local carrier density and the confining potential are found self-consistently by solving Poisson's equation coupled with the Schrödinger equation within the envelope function and effective mass framework.[20] The Poisson solver produces the electrostatic potential, in which the sub-band wave functions and energies (for Δ_2 and Δ_4 electrons as well as for holes) are found from the Schrödinger solver. The sub-bands are then populated according to the Fermi−Dirac distribution, and the resulting updated charge density is fed back into the Poisson solver. Iteration proceeds until satisfactory convergence is reached. The calculated Δ valley shift is the weighted average of the separation between the lowest Δ_2 and Δ_4 sub-band energies, according to their densities of states, which are proportional to the DOS effective mass for in-plane motion and the degeneracy of the valley. In Si(001), Δ_4 and Δ_2 contribute in the ratio $4(m_l m_t)^{1/2}$:$2m_t \approx 4.38$:1, while in Si(110) the contributions are in the ratio $4(m_t(m_t + m_l)/2)^{1/2}$:$2(m_l m_t)^{1/2} \approx 1.55$:1.

In the above, we used potential barriers of 3.15 and 4.05 eV for the CBM offsets at the Si/SiO_2 and H-terminated-Si/vacuum interfaces, respectively (see Methods). The difference in the barriers for these surface terminations has a negligible effect on the confinement-induced Δ-valley shift and splitting, because the barriers are so high and are similar in magnitude.

The above model gives the shift of the valleys and the positions of all the sub-bands within each valley, for a perfectly smooth slab. Those results are shown in Figure 2 for 2 and 5 nm thick membranes. In order to compare with experiment, we first introduce broadening of the DOS caused by outer-surface roughness. The roughness of this surface is caused by electromechanical polishing (part of the SOI fabrication process) and by our oxidation/etching thinning procedure. The outer-surface roughness is not correlated to the Si template/buried oxide interface because they were polished in independent steps. Additionally XAS is a quite local probe, measuring the local DOS in the vicinity of the atom on which the transition occurs.[21,22] For this uncorrelated roughness, therefore, the rms value over the size of the illuminated area is adequate to calculate broadening of sub-bands in each valley. In a Si sample of thickness t_s and rms roughness δ, an energy level E_n is broadened by a factor proportional to $(E_n\delta/t_s)^2$.[23] The roughness has a pronounced effect on the DOS (and hence ultimately on the XAS d*I*/d*E* curve), as shown in Figure 2. The higher-energy sub-bands of the

steplike DOS in a thin Si slab get washed out by roughness.

To determine the calculated absorption spectrum to compare to the XAS data, we must also include thermal broadening and lifetime broadening of the 2p core level (the energy width of the incident X-ray is negligible by comparison). We calculate the absorption spectrum, taking into account all transitions from 2p to the calculated quasi-2D electronic subbands in Δ_2 and Δ_4 as well as to the discrete excitonic levels.[24] We include thermal broadening and broadening due to the lifetime of the 2p level using a linear combination of Gaussian and Lorentzian functions.[25] The parameters that capture the cumulative effect of thermal broadening and the 2p lifetime were determined by fitting the calculated first derivative of the absorption spectrum (which is proportional to dI/dE in XAS) for the $2p_{3/2} \rightarrow \Delta$ transition in a 20 nm thick Si(001) membrane to the corresponding experimental peak. The 20 nm membrane X-ray absorption spectrum is indistinguishable from that of the bulk and shows negligible influence of surface roughness. These broadening parameters were then used to calculate the absorption spectrum for thinner samples, with the surface roughness included. Figure 3 shows the results. Figure 3a shows the DOS for a 5 nm thick membrane without roughness and the calculated XAS spectrum without roughness and with the experimental 0.4 nm rms roughness. Figure 3b shows that, of the mechanisms affecting the XAS spectrum, roughness is by far most important. Because of the pronounced roughness-induced suppression of all but the ground-state sub-band peak in each valley, the full $2p_{3/2} \rightarrow \Delta$ absorption peak is essentially the sum of peaks due to the lowest Δ_2 sub-band and the lowest Δ_4 sub-band. Whereas it is unfortunate that roughness suppresses all but the ground-state sub-band peaks, this fact allows us to determine splitting and shifting of the lowest Δ_2 sub-band and the lowest Δ_4 sub-band with reduced thickness of the membranes. Figure 4 shows the calculated derivatives of absorption spectra for several membrane thicknesses and a comparison with data. The relative contributions of the Δ_2 and Δ_4 peaks are well approximated by the ratio of their DOS, which justifies the procedure we use for extracting the Δ-valley shift and splitting from the XAS yield measurements. The $2p_{3/2} \rightarrow \Delta$ peak in the XAS spectra remains well resolved even for very thin membranes but visibly broadens with decreasing thickness.

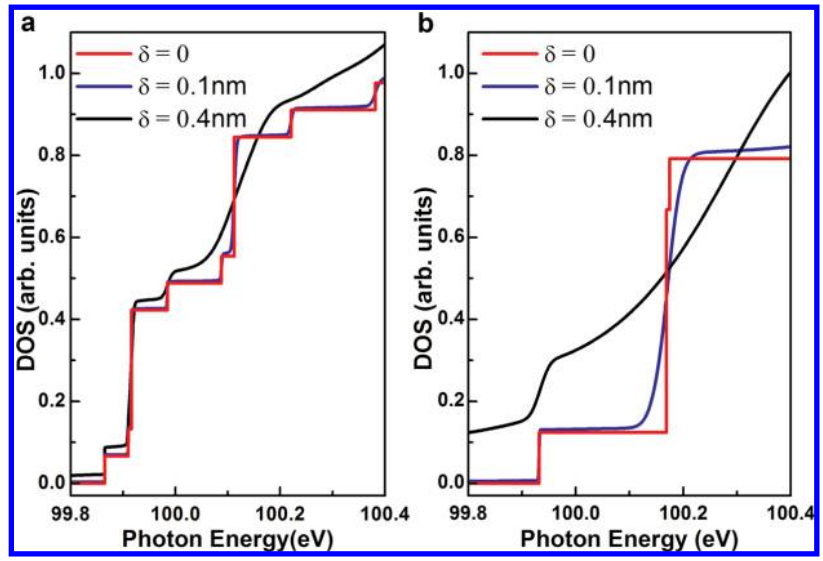

Figure 2. DOS for thin membranes and effect of roughness: (a) 5 nm thick membrane; (b) 2 nm thick membrane, both (001) orientation. The first large steps in the DOS correspond in both cases to the Δ_4 ground states, the first small steps correspond to Δ_2. The energy scale is chosen to correspond to the transition from the $2p_{3/2}$ core level of Si.

To determine the experimental value of valley splitting, we divide the 2p-to-Δ peak of bulk crystalline Si into contributions from Δ_2 and Δ_4.[9] For example, the Δ_2 and Δ_4 line shapes in bulk Si(001) are obtained by multiplying the full bulk line shape by $2m_t/(2m_t + 4(m_l m_t)^{1/2}) \approx 0.19$ and $4(m_l m_t)^{1/2}/(2m_t + 4(m_l m_t)^{1/2}) \approx 0.81$, respectively. The bulk line shapes of Δ_2 and Δ_4, obtained as above, are shifted independently and

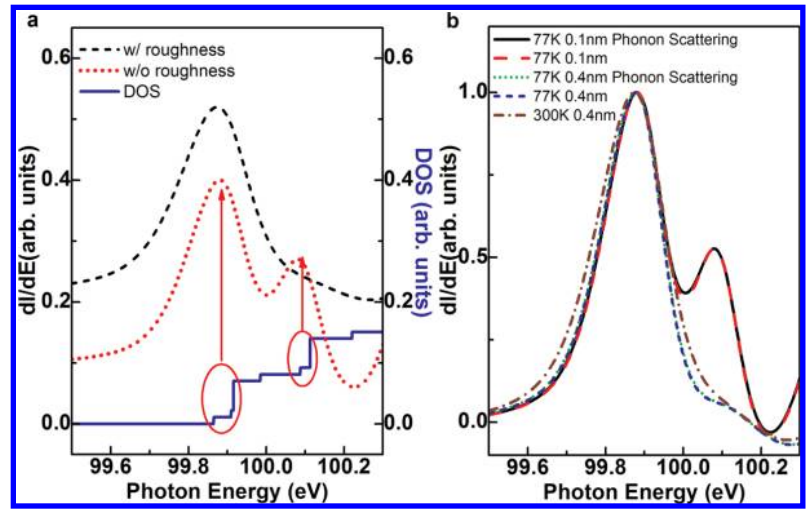

Figure 3. Calculated derivative of X-ray absorption spectra for the 2p-to-Δ transition for a 5 nm thick Si(001) membrane. (a) Modification of the spectrum by roughness: blue, DOS; red, zero roughness; black, with 0.4 nm roughness. Thermal and lifetime broadening are included. (b) Calculated absorption spectra for a 5 nm thick Si(001) membrane primarily at 77 K to reduce the thermal contribution, for two levels of roughness, 0.1 and 0.4 nm. The two curves with 0.1 nm roughness show an extra peak. All three curves with 0.4 nm roughness lack the peak, whether at 77 or 300 K. The dark red dash−dot curve is for 300 K. It is clear that roughness significantly modifies the spectrum.

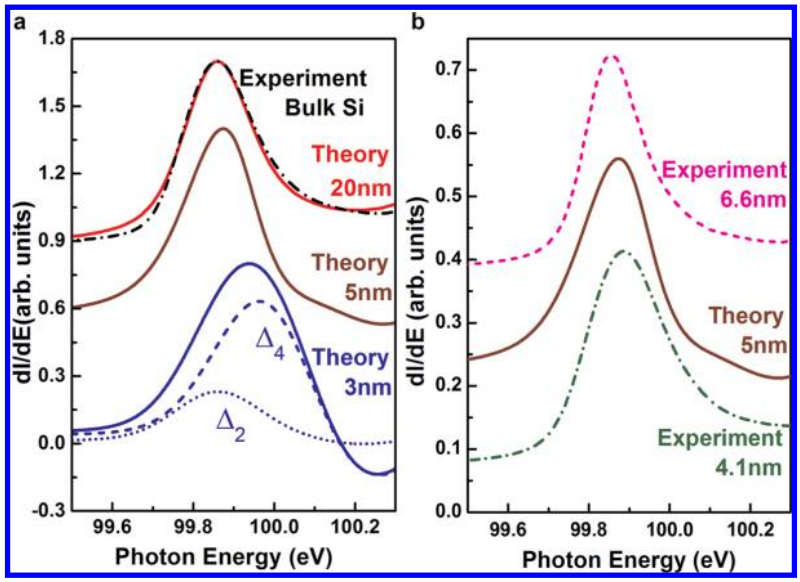

Figure 4. Calculated and measured derivative 2p-to-Δ absorption spectra for several membrane thicknesses. (a) Calculations at several thicknesses; 20 nm is the same as experimental bulk Si. The split Δ_2 and Δ_4 contributions to the peak for the 3 nm membrane are shown. The Δ_2 and Δ_4 peak separation increases with decreasing membrane thickness. (b) Comparison of the calculation for a 5 nm thick membrane with experiment for 4.1 and 6 nm thicknesses.

summed to obtain the best fit to the nanomembrane line shape for each thickness.

The $\Delta_2-\Delta_4$ splitting values obtained in this manner from the XAS measurements are in excellent agreement with our theoretical predictions, as shown in Figure 5 panels a and b for Si(001) and Si(110), respectively. The splitting can be over 250 meV. We find both experimentally and theoretically that, at the same Si layer thicknesses, Si(001) shows a larger ground state subband splitting than Si(110).

If we assume that the Si 2p energy level is localized and thus not influenced by membrane thickness, we can compare our experimental results of the (weighted) average energy shift of Δ valleys to the calculation. The results are shown as the solid lines in Figure 6a,b. The average shift can be more than 100 meV. The agreement between theory and experiment is very good down to very small thicknesses, at which the effective-mass and bulk-exciton approximations start to fail. Moreover, in contrast to the assumption in our calculation, the Si 2p core levels may shift somewhat with changing thickness, relative to the vacuum level.[26]

Strain can also shift and split levels.[27] There is evidence that the Si template layer contains a small amount of innate strain, perhaps as much as 0.3%,[28] because of the Si/oxide interface. On the basis of prior measurements[9] we can predict that this amount of strain contributes at most 15 meV to the splitting for the thinnest template layers, and less to the shift of the weighted average Δ valley energy. These possible contributions are small compared to the values measured here.

Efforts to extract the splitting of the Δ_2 and Δ_4 ground states in a quantum confined system have been made through interpretation of measurements of the electron mobility in a ultrathin channel SOI-based MOSFET.[29] Extracting information on conduction band splitting in quantum wells indirectly, through the electron mobility, can be affected by extrinsic parameters, such as electrical contacts and device layouts,[3] as well as by assumptions on the mobility behavior in confined

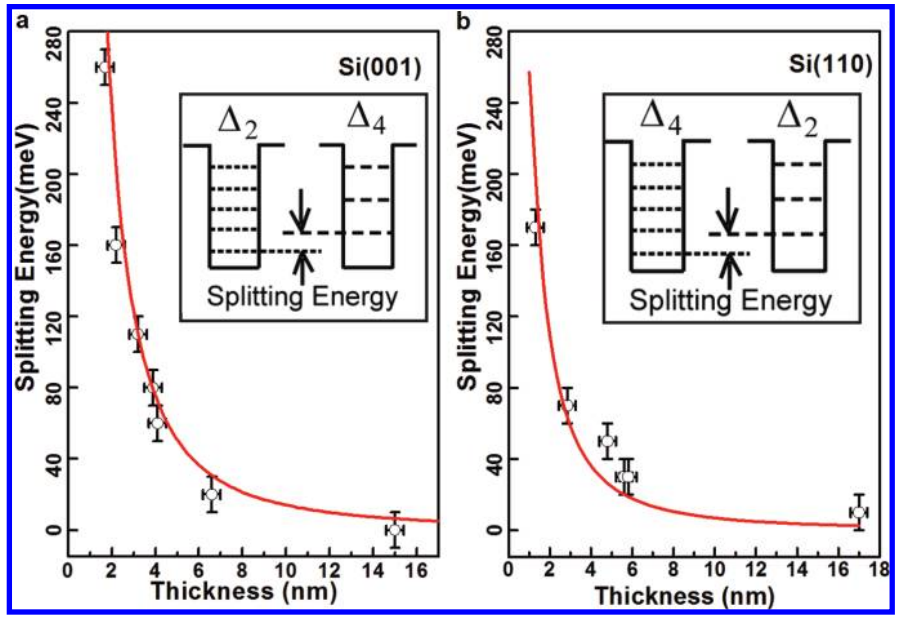

Figure 5. Quantum size effect: Splitting of the CBM as a function of the Si membrane thickness: (a) Si(001) and (b) Si(110). Symbols represent the measurements; solid lines represent the self-consistent calculation. The splitting is somewhat larger in Si(001) and the splitting of the valleys is reversed.

structures, which is in general quite complicated.[30,31] Such uncertainties inherent to transport measurement are absent in our direct measurement of the DOS *via* XAS. Our results may, in contrast, allow a determination of extrinsic influences on charge carrier mobility measurements.

We now extrapolate our results on 1D confined structures to 2D confined structures, i.e., nanowires. We have shown above, using roughnesses of 0.4 nm and an impossibly low 0.1 nm (a single-atomic-layer step in Si(001) is ~ 0.14 nm), that in nanomembranes (1D confinement) even small to moderate surfaces roughness modifies the DOS significantly. We project the effect of the same level of roughness onto the DOS of nanowires. For 2D confinement the DOS consists of sharp peaks rather than steps. We had hoped that roughness would have a weaker effect on the DOS, so that many more sub-bands could be observed and thus used in thermoelectric devices, as suggested by ref 32. Figure 7 shows the DOS for a 5 × 5 nm^2 wire[31] with no roughness and with 0.14 and 0.4 nm roughnesses. It is evident that even very low roughness modifies the DOS significantly and that moderate roughness destroys the ability to resolve higher-order minibands and severely diminishes the DOS of the lowest feature.

In the introduction we mentioned the prediction that quantum size effects could help the thermoelectric figure of merit by creating minibands that enhance the thermoelectric power factor $S^2\sigma$. (The power factor is a product of carrier conductivity σ and the square of the Seebeck coefficient S, and is the numerator in the thermoelectric figure of merit ZT, defined at temperature T as $ZT = (S^2\sigma/\kappa)T$; κ is thermal conductivity). We have demonstrated that even very small roughness washes out the sub-bands, so that making the wires very small does not produce improved electrical performance. The roughnesses required to reduce the thermal conductivity in Si nanowires[4,33,34] are quite large. Roughness in wires smaller than those that have been reported, although it may reduce the thermal conductivity further, has as a consequence of a much reduced electrical conductivity. Furthermore, the gain one hoped for in making sub-bands does not materialize because roughness destroys them.

At the small dimensions needed to take advantage of the quantum size effect there may be an optimal (very low) surface roughness that maximizes ZT while balancing the effect of a discrete band structure with low thermal conductivity. More promisingly, one could introduce high localized densities of states using heterostructures.[32,35,36] In group III−V materials, fabrication of heterostructures with significant band offsets in the appropriate directions is relatively straightforward.[37] In group IV materials it is not. Growing Si/Ge heterostructure nanowires does not allow a very high level of composition variation while maintaining crystallinity.[38] Furthermore, most of the band offset occurs in the valence band,[39] with the conduction band offsets relatively small. An alternative is a strain superlattice. It has recently been shown that, because of the sensitivity of the conduction band structure of Si to strain, large conduction band offsets are achievable[36] and miniband formation is possible using periodic local nanostressors.[35,36]

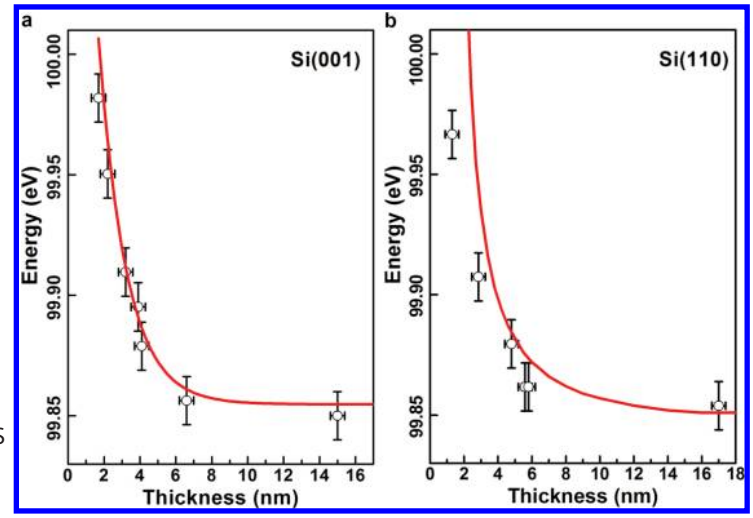

Figure 6. Quantum size effect: Shift of the weighted average Δ valley energy as a function of the Si membrane thickness: (a) Si(001) and (b) Si(110). Symbols represent the measurements; solid lines represent the self-consistent calculation.

Our results are also relevant in classical and quantum electronics. Quantum confinement increases the band gap; in field effect transistors based on ultrathin SOI, it therefore becomes harder to get an inversion layer—higher threshold voltages are required.[40] Our quantitative determination of the shift in the ground state sub-bands can be directly correlated with the threshold voltage increase.

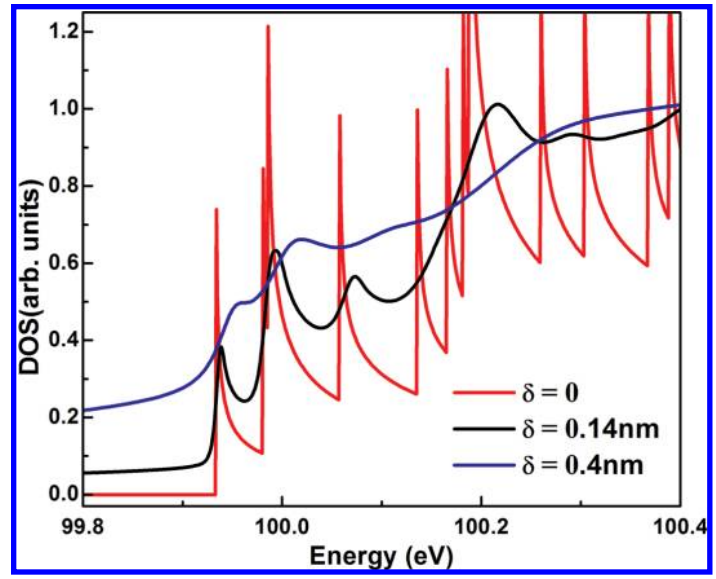

Figure 7. DOS of a 5 nm × 5 nm Si nanowire (red) and effect of two levels of surface roughness, 0.14 nm (black) and 0.4 nm (blue). The energy scale corresponds to the photon transition from the $2p_{3/2}$ core level.

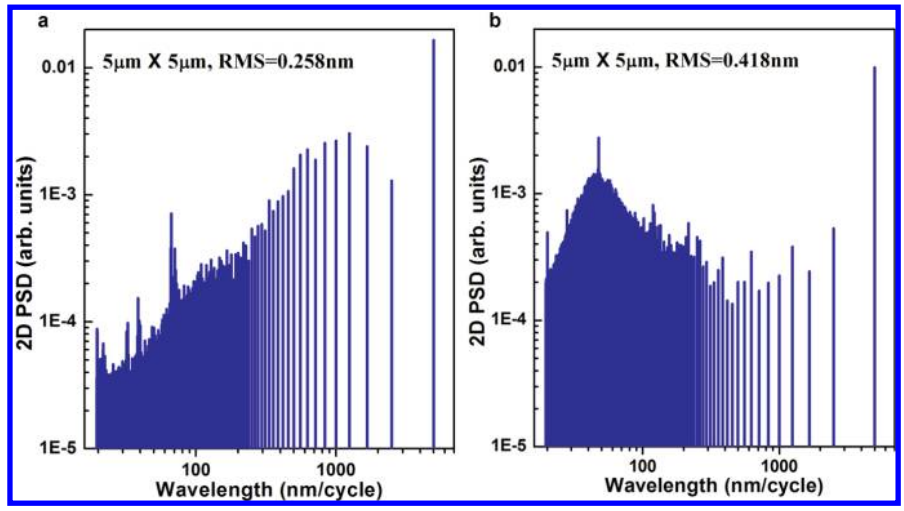

Figure 8. Two-dimensional power spectral density for two Si nanomembranes with different surface roughness: (a) rms = 0.258 nm; (b) rms = 0.418 nm. The scan area for both samples is 5 μm × 5 μm.

The smearing of the peaks in the DOS furthermore has implications for carrier coherence in quantum electronics and Si-based quantum information. When level splitting upon confinement becomes larger than the typical Brillouin-zone-end phonon energy (~60 meV in Si), intervalley phonon scattering becomes suppressed. As the densities of states of the split sub-bands are broadened by roughness, the "gap" between levels is effectively shrunk, meaning that the roughness indirectly enhances the rates for intervalley scattering, thereby diminishing the confinement-induced benefit. This roughness-induced enhancement of intervalley scattering has repercussions on silicon-based quantum information processing[41] as it increases the decoherence rate.

Ultimately, degeneracy splitting induced by strain appears to be more effective than that induced by confinement, as confinement necessarily implies that surface roughness becomes a factor and diminishes the benefits obtained by valley splitting.[13]

CONCLUSIONS

We have measured the dependence of the splitting and shifting of the conduction band Δ valleys in Si(001) and Si(110) on the degree of 1D spatial confinement and compared to self-consistent theory. The agreement is excellent. Measurements on extremely thin Si are made possible by the unique shallow probe depth of total-electron-yield detection in soft-X-ray absorption spectroscopy. A direct measurement of the Δ valley splitting due to quantum confinement has not been possible by other means. In contrast to electrical measurements, XAS enables a clear view of confinement-induced changes in the DOS alone.

We have explicitly included the effect of surface roughness and demonstrated its immense importance in modifying the DOS and the XAS spectra. Because of the significant interest in using Si nanostructures as thermoelectric materials, we have explored theoretically the extension of our results from 1D confinement to 2D confinement. It is quite clear that even small surface roughness seriously compromises the use of the quantum size effect in Si for enhancing the thermoelectric power factor and additionally influences charge carrier behavior relevant in classical and quantum electronics.

METHODS

Fabrication of Ultrathin Si Nanomembranes. Both SOI(001) and SOI(110) wafers are commercially obtained from Soitec. They have a 200 nm Si template layer on 150 nm buried oxide supported by a handle wafer. Nanomembrane preparation is described in detail in recent reviews.[42−44] Specifically, to reduce the thickness of the template layer, we use thermal oxidation at 1050 °C for 3.5 h. The thermal oxide is then stripped off in 6:1 buffered oxide etchant (BOE). After this thermal oxidation, ~15 nm of Si template layer remains. Small pieces of the wafer are cleaned in piranha (H_2SO_4 + H_2O_2), AHP (NH_4OH + H_2O_2, 80 °C), and diluted HF (12%). This wet-chemical-clean process has a rate of thickness reduction of as little as 2 nm per cycle. For plasma thinning, samples are rinsed in DI water, dried in nitrogen, and transferred to a plasma chamber. A CF_4+O_2 plasma operated at 40 mTorr is used to reduce the Si template layer to the desired thickness. This process is very controllable and the etching rate is stable to about 0.5 nm/second. The plasma etching increases surface roughness. If the top membrane is released from the oxide, flipped over, and measured with AFM, a rms roughness of 0.19 nm is determined, very similar to the value for bulk Si, as it should be.[42]

Membranes with the desired thickness are intentionally covered with oxide to protect the surface. Before XAS measurements, we dip all but the thinnest samples into dilute HF (12%) to remove the top oxide. These now H-terminated membranes are moved into the load-lock of the ultrahigh vacuum XAS chamber within 2 min. The surface of the very thinnest samples was left oxide-terminated, to avoid the formation of large holes that occurs in these very thin membranes with the final HF dip. The native oxide only reduces the electron yield relative to the H ter-

mination but changes nothing about the Si XAS spectral features of interest here.

Membrane thicknesses as low as 5 nm and as high as several hundred nanometers are measured by ellipsometry calibrated by X-ray diffraction. The thicknesses of thinner membranes are determined from the above measurements using the calibration of the plasma etch rate.[42] Atomic force microscopy (AFM) on widely separated areas shows a rms surface roughness (measured over 5 μm × 5 μm regions) of nanomembranes prepared in this manner as low as 0.27 nm and below 0.4 nm for all samples, uniformly in all areas. We use new tips, as the measured roughness is sensitive to roughness.[45] We used bulk Si(001), cleaned in the same manner, and amorphous Si, prepared by sputter deposition, as references in the XAS measurements. The roughness, in comparison, for these surfaces was 0.18 nm for bulk Si and 0.67 nm for amorphous Si. We also obtain power spectral densities (PSDs) of the surface roughness of the thin membranes. Two examples are shown in Figure 8. The frequencies are limited at the high end by tip shape and at the low end by the size of the scan.[46] As noted in the text, even though these PSDs are somewhat different, the nature of the XAS process allows us to use rms roughness.

XAS Characterization. The XAS measurements were made using the varied-line-space plane grating monochromator (VLS-PGM) beamline at the University of Wisconsin-Madison Synchrotron Radiation Center, with a home-built ultrahigh vacuum XAS chamber (bass pressure $= 1-3 \times 10^{-10}$ Torr). Linearly polarized X-rays with incident direction normal to the sample surface are generated from undulator magnets. The intensity is sufficient to allow use of the narrowest monochromator exit slit to select the desired photon energy. This approach minimizes the energy dispersion of the X-ray spot on the sample. The electron yield current is gathered by a picoammeter that is connected to the sample holder *via* an electrical feed-through. The final absorption spectra are normalized by the electron yield from a gold mesh that is placed in front of the sample, in order to compensate for the change in the beam intensity due to fluctuations of the X-ray intensity during data collection, and also for the optical characteristics of the monochromator. Variation in such normalized XAS spectra are significantly reduced compared to the as-collected spectra. Only room-temperature or above operation is possible in the chamber; hence we are not able to explore potential changes in the spectra as the thermal broadening is reduced, as hinted at in the calculations shown in Figure 3b.

Acknowledgment. This research is supported by DOE, Grant No. DE-FG02-03ER46028, by NSF/MRSEC program (DMR-0520527), and by AFOSR (FA9550-09-1-0230). Facilities support from NSF/MRSEC is also acknowledged. The UW-Madison Synchrotron Radiation Center is supported by NSF Grant No. DMR-0537588. F. Chen is supported by the Chinese Scholar Council (CSC). C. Euaruksakul has been supported by a Thai government fellowship.

REFERENCES AND NOTES

1. Sanders, G. D.; Stanton, C. J.; Chang, Y. C. Y. C. Theory of Transport in Silicon Quantum Wires. *Phys. Rev. B* **1993**, *48*, 11067–11076.
2. Wang, J. F.; Gudiksen, M. S.; Duan, X. F.; Cui, Y.; Lieber, C. M. Highly Polarized Photoluminescence and Photodetection from Single Indium Phosphide Nanowires. *Science* **2001**, *293*, 1455–1457.
3. Takagi, S.; Koga, J.; Toriumi, A. Mobility Enhancement of SOI MOSFETs Due to Subband Modulation in Ultrathin SOI Films. *Jpn J. Appl. Phys.* **1998**, *37*, 1289–1294.
4. Hochbaum, A. I; Chen, R. K.; Delgado, R. D.; Liang, W. J.; Garnett, E. C.; Najarian, M.; Majumdar, A.; Yang, P. D. Enhanced Thermoelectric Performance of Rough Silicon Nanowires. *Nature* **2008**, *451*, 163–167.
5. Boukai, A. I.; Bunimovich, Y.; Tahir-Kheli, J.; Yu, J. -K; Goddard Iii, W. A.; Heath, J. R. Silicon Nanowires as Efficient Thermoelectric Materials. *Nature* **2008**, *451*, 168–171.
6. Hicks, L. D.; Dresselhaus, M. S. Effect of Quantum-Well Structures on the Thermoelectric Figure of Merit. *Phys. Rev. B* **1993**, *47*, 12727–12731.
7. Hicks, L. D.; Dresselhaus, M. S. Thermoelectric Figure of Merit of A One-dimensional Conductor. *Phys. Rev. B* **1993**, *47*, 16631–16634.
8. Himpsel, F. J.; McFeely, F. R.; Morar, J. F.; Taleb-Ibrahimi, A.; Yarmoff, J. A. *Photoemission and Absorption Spectroscopy of Solids and Interfaces with Synchrotron Radiation*; Campagna, M., Rosei, R., Eds.; North Holland: Amsterdam, 1990; pp 203.
9. Euaruksakul, C; Li, Z. W.; Zheng, F.; Himpsel, F. J.; Ritz, C. S.; Tanto, B.; Savage, D. E.; Liu, X. S.; Lagally, M. G. Influence of Strain on the Conduction Band Structure of Strained Silicon Nanomembranes. *Phys. Rev. Lett.* **2008**, *101*, 147403-1–4.
10. Lu, Z. H.; Lockwood, D. J.; Baribeau, J. M. Quantum Confinement and Light-Emission in SiO_2/Si Superlattices. *Nature* **1995**, *378*, 258–260.
11. van Buuren, T.; Dinh, L. N.; Chase, L. L.; Siekhaus, W. J.; Terminello, L. J. Changes in the Electronic Properties of Si Nanocrystals as a Function of Particle Size. *Phys. Rev. Lett.* **1998**, *80*, 3803–3806.
12. Nishida, M. Quantum Confinement Effects on the Electronic Structure of Si(001) Ultrathin Films: Energy Shifts of Optical Band Edges and Luminescence in Crystalline and Amorphous Si Films. *Phys. Rev. B* **1999**, *59*, 15789–15795.
13. Euaruksakul, C.; Chen, F.; Tanto, B.; Ritz, C. S.; Paskiewicz; D, M.; Himpsel, F. J.; Savage, D. E.; Zheng, L.; Yao, Y. G.; Liu, F.; *et al. Phys. Rev. B* **2009**, *80*, 115323-1–11.
14. Morar, J. F.; Batson, P. E.; Tersoff, J. Heterojuction Band Lineups in SiGe Alloys Using Spatially Resolved Electron-Energy-Loss Spectroscopy. *Phys. Rev. B* **1998**, *47*, 4107–4110.
15. Huang, L. J.; Lau, W. M.; Tang, H. T.; Lennard, W. N.; Mitchell, I. V.; Schultz, P. J.; Kasrai, M. Near-Surface Structure of Low-Energy-Argon-Bombarded Si(100). *Phys. Rev. B* **1994**, *50*, 18453–18468.
16. Savitzky, A.; Golay, M. J. E. Smoothing and Differentiation of Data by Simplified Least Squares Procedures. *Anal. Chem.* **2002**, *36*, 1627–1639.
17. Faleev, S. V.; van Schilfgaarde, M.; Kotani, T. All-Electron Self-Consistent GW Approximation: Application to Si, MnO, and NiO. *Phys. Rev. Lett.* **2004**, *93*, 126406–126409.
18. Chiang, T. C.; Himpsel, F. J. *Landolt-Börnstein—Group III Condens. Matter* **2006**, *23a*, 15.
19. Batson, P. E.; Heath, J. R. Electron Energy Loss Spectroscopy of Single Silicon Nanocrystals: The Conduction Band. *Phys. Rev. Lett.* **1993**, *71*, 911–914.
20. Knezevic, I.; Ramayya, E. B.; Vasileska, D.; Goodnick, S. M. Diffusive Transport in Quasi-1D and Quasi-2D Electron Systems. *J. Comput. Theor. Nanosci.* **2009**, *6*, 1725–1753.
21. Ramaker, D. E.; Murday, J. S.; Turner, N. H.; Moore, G.; Lagally, M. G.; Houston, J. Calculated and Measured Auger Line-Shape in SiO_2. *Phys. Rev. B* **1979**, *19*, 5375–5387.
22. Saldin, D. K. The Theory of Electron Energy-Loss Near-Edge Structure. *Philos. Mag. B* **1987**, *56*, 515–525.
23. Jin, S. H.; Fischetti, M. V.; Tang, T. W. Modeling of Surface-Roughness Scattering in Ultrathin-Body SOI MOSFETs. *IEEE Trans. Electron Dev.* **2007**, *54*, 2191–2203.
24. Chuang S. L. *Physics of Optoelectronic Devices*; Wiley-Interscience: New York, 1995; pp 124—141.
25. Bozek, J. D.; Bancroft, G. M.; Cutler, J. N.; Tan, K. H. Vibrationally Resolved Core-Level Photoelectron Spectroscopy: Si 2p Levels of SiH_4 and SiF_4 Molecules. *Phys. Rev. Lett.* **1990**, *65*, 2757–2760.
26. Chen, T. P.; Liu, Y.; Sun, C. Q.; Tse, M. S.; Hsieh, J. H.; Fu, Y. Q.; Liu, Y. C.; Fung, S. Core-Level Shift of Si Nanocrystals Embedded in a SiO_2 Matrix. *J. Phys. Chem. B* **2004**, *108*, 16609–16612.
27. Fischetti, M. V.; Laux, S. E. Band Structure, Deformation Potentials, and Carrier Mobility in Strained Si, Ge, and SiGe Alloys. *J. Appl. Phys.* **1996**, *80*, 2234–2252.

28. Tiberj, A.; Fraisse, B.; Blanc, C.; Contreras, S.; Camassel, J. Process-Induced Strain in Silicon-on-Insulator Materials. *J. Phys.: Condens. Matter* **2002**, *14*, 13411–13416.
29. Tsutsui, G.; Hiramoto, T. Experimental Study on Mobility in (110)-Oriented Ultrathin-Body Silicon-on-Insulator *n*-Type Metal Oxide Semiconductor Field-Effect Transistor with Single- and Double-Gate Operations. *Jpn. J. Appl. Phys.* **2007**, *46*, 5686–5690.
30. Ramayya, E. B.; Vasileska, D.; Goodnick, S. M.; Knezevic, I. Electron Mobility in Silicon Nanowires. *IEEE Trans. Nanotechnol.* **2007**, *6*, 113–117.
31. Ramayya, E. B.; Vasileska, D.; Goodnick, S. M.; Knezevic, I. Electron Transport in Silicon Nanowires: The Role of Acoustic Phonon Confinement and Surface Roughness Scattering. *J. Appl. Phys.* **2008**, *104*, 063711−063712.
32. Lin, Y.-M.; Dresselhaus, M. S. Thermoelectric Properties of Superlattice Nanowires. *Phys. Rev. B* **2003**, *68*, 075304−1-14.
33. Chen, R.; Hochbaum, A. I.; Murphy, P.; Moore, J.; Yang, P. D.; Majumdar, A. Thermal Conductance of Thin Silicon Nanowires. *Phys. Rev. Lett.* **2008**, *101*, 105501–105504.
34. Martin, P.; Aksamija, Z.; Pop, E.; Ravaioli, U. Impact of Phonon-Surface Roughness Scattering on Thermal Conductivity of Thin Si Nanowires. *Phys. Rev. Lett.* **2009**, *102*, 125503-1−4.
35. Yu, D.; Zhang, Y.; Liu, F. First-Principles Study of Electronic Properties of Biaxially Strained Silicon: Effects on Charge Carrier Mobility. *Phys. Rev. B* **2008**, *78*, 245204-1−8.
36. Huang, M. -H.; Ritz, C. S.; Novakovic, B.; Yu, D. C.; Zhang, Y.; Flack, F.; Savage, D. E.; Evans, P. G.; Knezevic, I.; Liu, F.; *et al*. Mechano-electronic Superlattices in Silicon Nanoribbons. *ACS Nano* **2009**, *3*, 721–727.
37. Fuhrer, A.; Froberg, L. E.; Pedersen, J. N.; Larsson, M. W.; Wacker, A.; Pistol, M. E.; Samuelson, L. Few Electron Double Quantum Dots in InAs/InP Nanowire Heterostructures. *Nano Lett.* **2007**, *7*, 243–246.
38. Xiang, J.; Lu, W.; Hu, Y. J.; Wu, Y.; Yan, H.; Lieber, C. M. Ge/Si Nanowire Heterostructures as High-Performance Field-Effect Transistors. *Nature* **2006**, *441*, 489–493.
39. Yu, E. T.; Croke, E. T.; McGill, T. C.; Miles, R. H. Measurement of the Valence-Band Offset in Strained Si/Ge(100) Heterojunctions by X-ray Photoelectron-Spectroscopy. *Appl. Phys. Lett.* **1990**, *56*, 569–571.
40. Knezevic, I.; Vasileska, D. Z.; Ferry, D. K. Impact of Strong Quantum Confinement on the Performance of a Highly Asymmetric Device Structure: Monte Carlo Particle-Based Simulation of a Focused-Ion-Beam MOSFET. *IEEE Trans. Electron Devices* **2002**, *49*, 1019–1026.
41. Goswami, S.; Slinker, K. A.; Friesen, M.; McGuire, L. M.; Truitt, J. L.; Tahan, C.; Klein, L. J.; Chu, J. O.; Mooney, P. M.; van der Weide, D. W.; *et al*. Controllable Valley Splitting in Si/SiGe Quantum Devices. *Nat. Phys.* **2007**, *3*, 41–45.
42. Scott, A.; Peng, W. N.; Kiefer, A. M.; Jiang, H. Q.; Knezevic, I.; Savage, D. E.; Eriksson, M. A.; Lagally, M. G. Influence of Surface Chemical Modification on Charge Transport Properties in Ultrathin Silicon Membranes. *ACS Nano* **2009**, *3*, 1683–1692.
43. Cavallo, F.; Lagally, M. G. Semiconductors Turn Soft: Inorganic Nanomembranes. *Soft Matter* **2009**, *6*, 439–455.
44. Scott, S. A.; Lagally, M. G. Elastically Strain-Sharing Nanomembranes: Flexible and Transferable Strained Silicon and Silicon−Germanium Alloys. *J. Phys. D* **2007**, *40*, R75–R92.
45. Larsen, T.; Moloni, K.; Flack, F.; Eriksson, M. A.; Lagally, M. G.; Black, C. T. Comparison of Wear Characteristics of Etched-Silicon and Carbon Nanotube Atomic-Force Microscopy Probes. *Appl. Phys. Lett.* **2002**, *80*, 1996–1998.
46. Teichert, C.; MacKay, J. F.; Savage, D. E.; Lagally, M. G.; Brohl, M.; Wagner, P. Comparison of Surface Roughness of Polished Silicon Wafers Measured by Light Scattering Topography, Soft-X-ray Scattering, and Atomic-Force Microscopy. *Appl. Phys. Lett.* **1995**, *66*, 2346–2348.